EWEA, Special Topic Conference 2004: The Science of Making Torque from the Wind, Delft, April 19-21, 2004, pp. 546-555.
SAND2011-8343C

The Effect of Mean Stress on Damage Predictions for Spectral Loading of Fiberglass Composite Coupons[1]

Herbert J. Sutherland
Sandia National Laboratories
Albuquerque, NM 87185-0708
hjsuthe@sandia.gov

John F. Mandell
Montana State University
Bozeman, MT 59717
johnm@coe.montana.edu

Abstract:

In many analyses of wind turbine blades, the effects of mean stress on the determination of damage in composite blades are either ignored completely or they are characterized inadequately. Mandell, et al [1] have recently presented an updated Goodman diagram for a fiberglass material that is typical of the materials used in wind turbine blades. Their formulation uses the MSU/DOE Fatigue Data Base [2] to develop a Goodman diagram with detailed information at thirteen R-values. Using these data, linear, bi-linear and full Goodman diagrams are constructed using mean and "95/95" fits to the data. The various Goodman diagrams are used to predict the failure stress for coupons tested using the WISPERX spectrum [3]. Three models are used in the analyses. The first is the linear Miner's rule commonly used by the wind industry to predict failure (service lifetimes). The second is a nonlinear variation of Miner's rule which computes a nonlinear Miner's Sum based upon an exponential degradation parameter. The third is a generalized nonlinear residual strength model that also relies on an exponential degradation parameter. The results illustrate that Miner's rule does not predict failure very well. When the mean Goodman diagram is used, the nonlinear models predict failures near the mean of the experimental data, and when the 95/95 Goodman diagram is used, they predict the lower bound of the measured data very well.

Keywords: wind, blades, fatigue, spectral, fiberglass.

1 Introduction

In many analyses of wind turbine blades, the effects of mean stress on the determination of damage in composite blades are either ignored completely or they are characterized inadequately. Mandell, et al [1] have recently presented an updated characterization of the fatigue properties for fiberglass materials that are typically used in wind turbine blades. Their formulation uses the MSU/DOE Fatigue Data Base [2] and a three-parameter model to describe the mean S-N behavior of the fiberglass at thirteen different R-values. The R-value for a fatigue cycle is defined as:

$$R = \frac{\sigma_{min}}{\sigma_{max}} \quad , \tag{1}$$

where σ_{min} is the minimum stress and σ_{max} is the maximum stress in a fatigue stress cycle (tension is considered positive and compression is negative).

The results are typically presented as a Goodman diagram in which the cycles-to-failure are plotted as a function of mean stress and amplitude along lines of constant R-values. This diagram is the most detailed to date, and it includes several loading conditions that have been poorly represented in earlier studies.

This formulation allows the effects of mean stress on damage calculations to be evaluated. Using field data from the Long term Inflow and Structural Test (LIST) program, Sutherland and Mandell [4] have shown that the updated Goodman diagram predicts longer service lifetimes and lower equivalent fatigue loads than previous analyses. This prediction is a direct result of the lower damage predicted for the high-mean-stress fatigue cycles as a result of using the updated Goodman diagram.

To validate this result in a controlled set of experiments, the spectral loading data of Wahl et al [5] is evaluated using the updated Goodman diagram. These data are from coupons that were tested to failure using the WISPERX spectrum [3]. Six formulations for the S-N behavior of fiberglass are used: the first three use mean fits of the S-N data to construct a linear, bi-linear and full (13 R-values) Goodman diagram and the second three using "95/95" fits to construct similar diagrams (the 95/95 fit implies that, with a 95 percent level of confidence, the material will meet or exceed this design value 95

[1] *Sandia is a multiprogram laboratory operated by Sandia Corporation, a Lockheed Martin company, for the U.S. Department of Energy under contract DE-AC04-94AL85000

percent of the time). These formulations of the Goodman diagram are used with Miner's Rule and two non-linear residual strength models to predict the measured lifetime of the coupons.

2 Fatigue Data

The DOE/MSU fatigue database[2] contains over 8800 test results for over 130 material systems [2]. The database contains information on composite materials constructed from fiberglass and carbon fibers in a variety of matrix materials that are typically used in wind turbine applications. References 2, 6 and 7 provide a detailed analysis of data trends and blade substructure applications.

Recent efforts to improve the accuracy of spectrum loading lifetime predictions for fiberglass composites have led to the development of a more complete Goodman diagram than previously available.

2.1 Constant Amplitude Data

The material under consideration here is a typical fiberglass laminate that is called DD-16 in the DOE/MSU Database. This laminate has a $[90/0/\pm45/0]_S$ configuration with a fiber volume fraction of 0.36. The 90° and 0° plies are D155 stitched unidirectional fabric, the ±45° plies are DB120 stitched fabric, and the resin is an ortho-polyester. Mandell et al [2, 5] described the test methodologies used to obtain the data cited here. This material has a static tensile strength of 625 MPa and a compressive strength of 400 MPa. The 95/95 strength values are 510 MPa and 357 MPa, respectively. These strength values were determined at a strain rate similar to that of the fatigue tests.

For illustrative purposes, the constant amplitude data at R = –1, 0.1 and 10 are shown in Fig. 1. A complete set of the data for all thirteen R-values is available in Refs. 1 and 2.

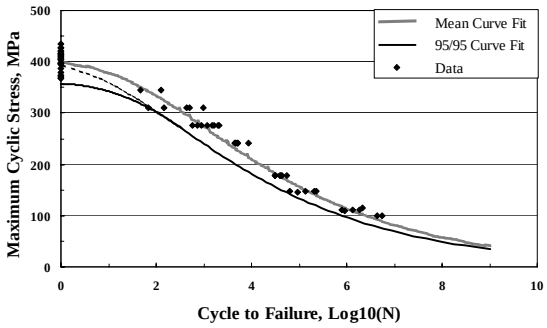

Figure 1a: R= –1.

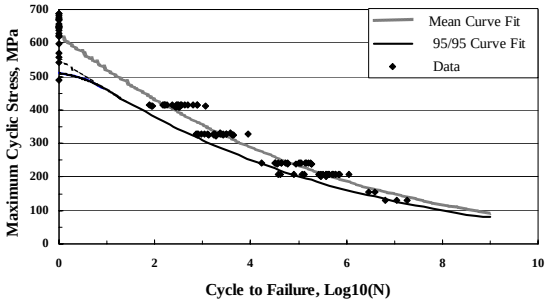

Figure 1b: R=0.1

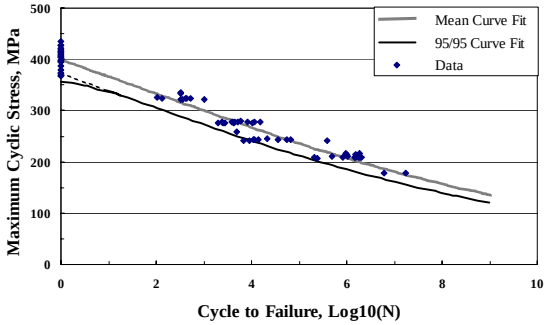

Figure 1c: R= 10

Figure 1: S-N Curves at Three R-Values for Database Material DD-16

2.1.1 Curve Fits

2.1.1.1 Mean Fit

As presented by Mandell et al [1], the constant amplitude data at 13 R-values were fit with a three-parameter equation of the following form:

$$\sigma_O - \sigma = a\sigma \left[\frac{\sigma}{\sigma_O}\right]^b (N^c - 1) \quad , \tag{2}$$

where σ is the maximum applied stress, σ_O is the ultimate tensile or compressive strength (obtained at a strain rate similar to the 10 Hz fatigue tests), N is the mean number of constant-amplitude cycle to failure, and a, b, and c are the fitting parameters. The results of these fits are summarized in the Table and illustrated in Fig. 1.

[2] The database is available on the SNL website: http://www.sandia.gov/wind/.

The parameters in these curve fits were selected to provide the best fit to the experimental data and to provide a 10^9 cycle extrapolation stress which was within ten (10) percent of the extrapolation from a simple two-parameter power law fit to the fatigue data having lifetimes greater than 1000 cycles [1].

2.1.1.2 95/95 Fit

Using the techniques cited in Ref. 8 and 9 and the "Standard Practice" cited in Ref. 10, the 95/95 curve fits were also determined for these data. The 95/95 fit implies that, with a 95 percent level of confidence, the material will meet or exceed this design value 95 percent of the time.

For these calculations, we use a one-sided tolerance limit, which has been computed and tabulated for several distributions by a number of authors. Typically, these tabulations take the following form:

$$X^* = \overline{X} - c_{1-\alpha,\gamma}\, X_x \quad , \tag{3}$$

where $\overline{X}$ and X_X. are the sample average and the standard deviation, respectively. The parameter $c_{1-\alpha,\gamma}$ is tabulated as a function of the confidence level $(1-\alpha)$, probability γ and the number of data points n.

For fatigue fits, the independent variable is the stress σ and the dependent variable is the logarithm of the number of cycles to failure N. Thus, the sample average is the $\log_{10}(N)$ determined from Eq. 2 and the standard deviation X_X is given by:

$$X_x = \left[\frac{\sum_{i=1}^{n}\left(X_i - \overline{X}\right)^2}{(n-1)}\right]^{\frac{1}{2}} = \left[\frac{\sum_{i=1}^{n}\left\{\log_{10}\left[N_i(\sigma_i)\right] - \log_{10}\left[N(\sigma_i)\right]\right\}^2}{(n-1)}\right]^{\frac{1}{2}} . \tag{4}$$

Thus, the number of cycles to failure for the 95/95 fit is given by:

$$\log_{10}\left[N_{95/95}\right] = \log_{10}\left[N\right] - \log_{10}\left[N_o\right] \quad , \tag{5}$$

where $\log_{10}[N_o]$ is tabulated for each of the thirteen R-values in the Table.

As shown in Fig. 1, this technique works well for the fatigue data. However, this technique does not yield the 95/95 static strength that is determined from static strength data, see the dotted lines in the figure. To rectify this situation, the 95/95 fatigue curve was "faired" into the measured 95/95 static strength, as shown by the solid lines in the figure [11].

Table: Parameters for the Thirteen R-Values for Material DD16 and for Small Strands

R-Value	Model (Equation 2)			95/95 (Equation 5)
	a	b	c	$\log_{10}(N_o)$
1.1	0.06	3	0.05	4.43
1.43	0.06	3	0.15	1.85
2	0.06	4	0.25	2.67
10	0.1	4	0.35	0.87
–2	0.01	4	0.55	0.59
–1	0.02	3	0.62	0.53
–0.5	0.45	0.85	0.25	0.64
0.1	0.42	0.58	0.18	0.70
0.5	0.075	2.5	0.43	0.79
0.7	0.04	2.5	0.45	0.65
0.8	0.035	2.5	0.4	0.79
0.9	0.06	2.5	0.28	1.20
1*	0.21	3	0.14	3.03

*Assumes a frequency of 10 Hz.

2.1.2 Goodman Diagrams

For the analysis of S-N data, the preferred characterization is the Goodman diagram. In this formulation, the cycles-to-failure are plotted as functions of mean stress and amplitude along lines of constant R-values. Between R-value lines, the constant cycles-to-failure plots are typically, but not always, taken to be straight lines.

Various Goodman diagrams for the DD-16 fiberglass composite are shown in Figs. 2 and 3. These figures are presented in increasing level of knowledge about the S-N behavior of the fiberglass composite material. Figures 2a and 3a illustrate the "linear" Goodman diagram. In these two figures, the diagrams are constructed using the static strength values for the tensile and compressive intercepts of the constant life curves with the horizontal axis of the diagram and the S-N data for the R = –1 (see Fig. 1a) for the intercepts of the vertical axis. The "bi-linear" Goodman diagrams, shown in Figs. 2b and 3b, are constructed by adding the R = 0.1 S-N data (see Fig. 1b) to the diagram. The "full" Goodman diagrams, shown in Figs. 2c and 3c, are constructed by adding the data for the remaining eleven R-values.

2.1.2.1 Mean Goodman Diagrams

The Goodman diagrams shown in Fig. 2 were constructed using Eq. 2 and the information in the Table. Figures 2a and 2b, use the mean static strengths for the intercepts of the constant-life curves

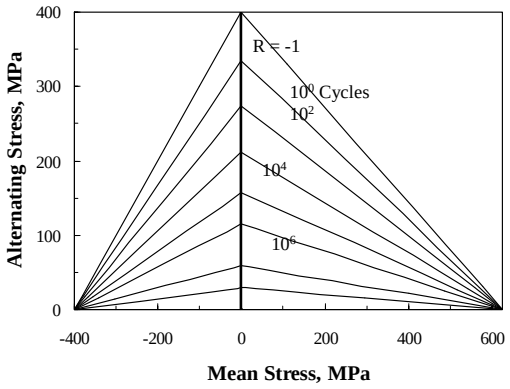

Fig. 2a: Linear Goodman Diagram

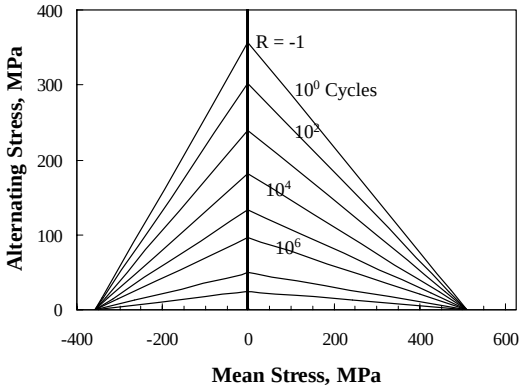

Fig. 3a: Linear Goodman Diagram

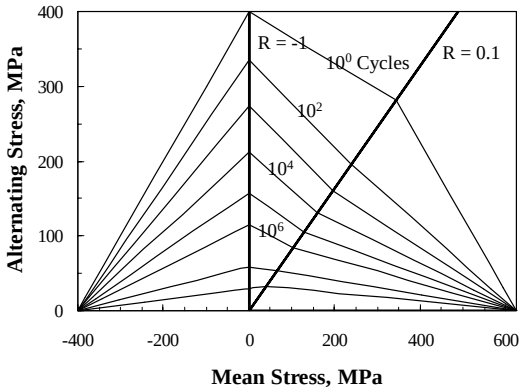

Fig. 2b: Bi-Linear Goodman Diagram

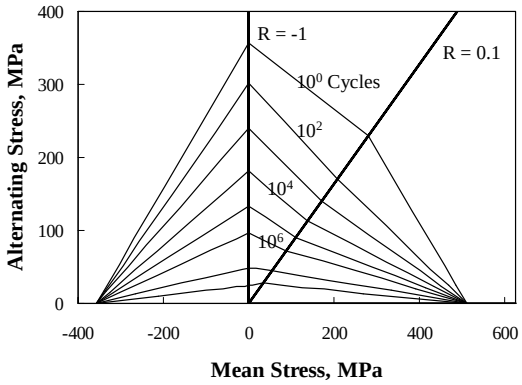

Fig. 3b: Bi-Linear Goodman Diagram

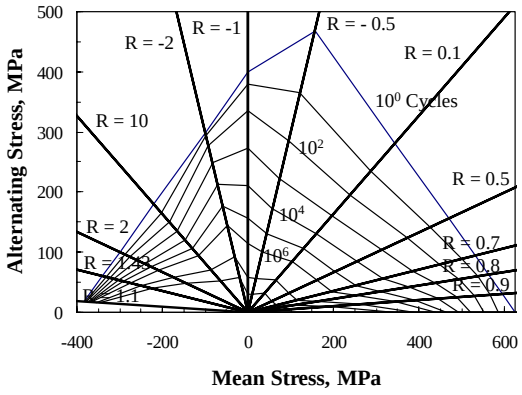

Fig. 2c: Full Goodman Diagram

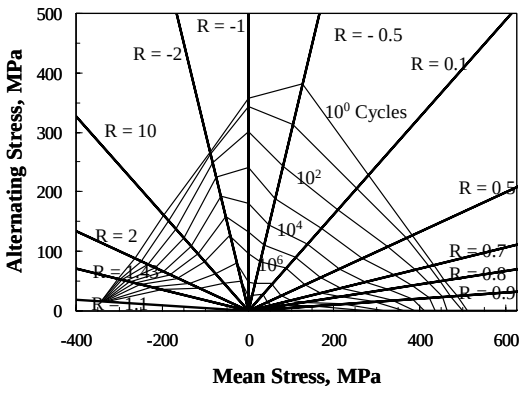

Fig. 3c: Full Goodman Diagram

Fig. 2. Mean Goodman Diagrams for Database Material DD16, Fit with Eq. 2

Fig. 3. 95/95 Goodman Diagrams for Database Material DD16, Fit with Eqs. 2 and 3

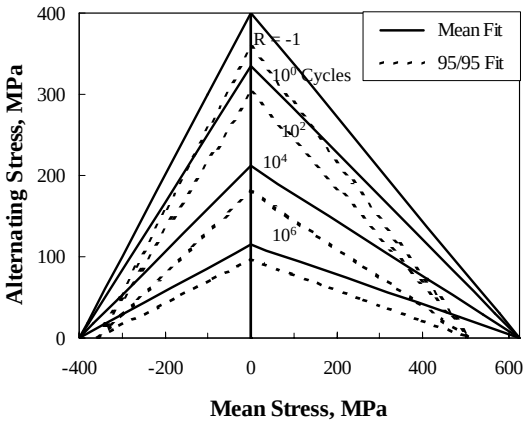

Fig. 4a: Linear Goodman Diagram

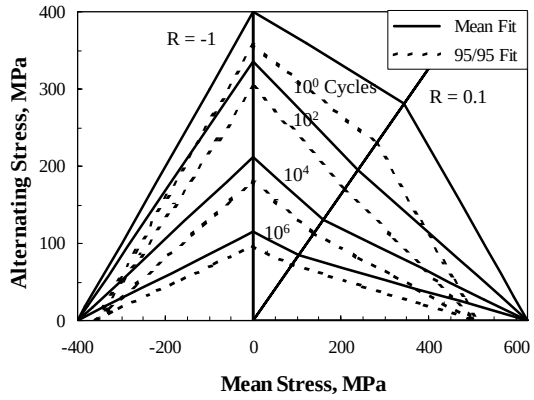

Fig. 4b: Bi-Linear Goodman Diagram

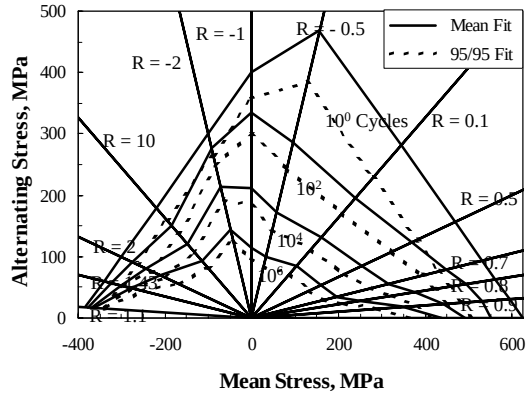

Fig. 4c: Full Goodman Diagram

Fig. 4: Comparison of Mean and 95/95Goodman Diagrams

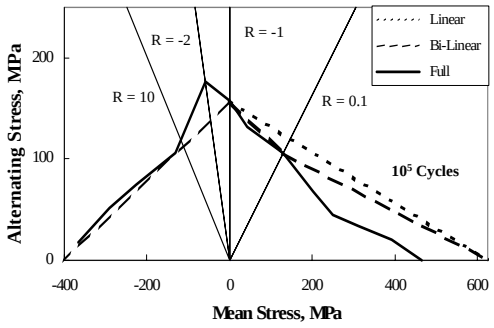

Fig. 5: Comparison of the Three Goodman Diagrams at 10^5 Cycles

with the mean stress (horizontal) axis. Fig. 2c departs from traditional formulations in that the intercept for tensile mean axis (R = 1) is not the mean static strength. Rather, the intercept is a range of values based upon time-to-failure under constant load. These data were converted to cycles by assuming a frequency of 10 cycles/second, typical of the cyclic tests. Nijssen et al [12] have hypothesized a similar formulation previously.

2.1.2.2 95/95

The Goodman diagrams cited in Fig. 3 were constructed using Eqs. 2 and 6, the information in the Table, and the fairing of the S-N curves into the 95/95 static strengths. Again, the tensile intercept in Fig. 3c is a range of values based upon time under load.

2.1.2.3 Comparison

The Goodman diagrams presented in Figs. 2 and 3 are compared with one another in Figs. 4 and 5.

As shown in Fig. 4, the general shapes of the various Goodman diagrams are unchanged by conversion from the mean values to the 95/95 values.

The significant differences in the Goodman formulations are highlighted in Fig. 5. The area near the R = –1 axis is very important. This is the region where the fiberglass composite is in transition between compressive and tensile failure modes and many of the stress cycles on a wind turbine blade have an R-value near –1. The effect of the mode change on fatigue properties is illustrated by the direct comparison of the constant life curves for the three Goodman diagrams. In Fig. 5, the constant life curves for the three formulations of the Goodman diagram at 10^5 cycles are compared to one another. Four distinct regions of comparison are noted: (1) the region of relatively high compressive mean stress ($1< R < \infty$, i.e., essentially the region to the left of R = 10); (2) the

region of relatively low compressive stress ($-\infty < R < -1$; i.e., essentially the region between R = 10 and R = 1); (3) the region of relatively low tensile stress ($-1 < R < 0$; i.e., essentially the region between R = –1 and R = 0.1); and (4) the region of relatively high tensile stress ($1 < R < 0$; i.e., essentially the region to the right of R = 0.1). In the first and third regions, the three formulations lie close to one another. Thus, each of the three formulations will predict approximately the same damage rate for the stress cycles in this range. For the fourth region (high tensile stress) the database formulation is below the linear and bi-linear formulations. Thus, the database formulation is more severe (i.e., it produces a shorter predicted service lifetime) than the other two. And, finally, for the second region (low compressive stress), the database formulation is above the linear and bi-linear formulations. Thus, it is less severe. Regions 2 and 3 are where the composite is in transition between compressive and tensile failure modes.

2.2 WISPERX Spectral Data

Wahl et al [5] have conducted spectral loading tests of coupons using the WISPERX spectrum [3]. The WISPERX spectrum is the WISPER spectrum with the small amplitude fatigue cycles removed. The WISPERX spectrum, see Fig. 6, consists of over 25,000 peaks-and-valleys (load reversal points) or slightly over 10^4 cycles. The original formulation of the spectrum is in terms of load levels that vary from 0 to 64 with zero at load level 25. When normalized to the maximum load in the spectrum, the load levels take the values shown in the figure. The minimum load level is –0.6923 and, of course, the maximum load level is 1.0.

Figure 6 illustrates that the WISPERX spectrum is primarily a tensile spectrum with a relatively small number of compressive cycles.

3 Damage Models

Typically, the wind industry uses Miner's rule to estimate damage under spectral loads. Many other models for damage estimation have been proposed. Two, which are investigated here, are the nonlinear Miner's Sum proposed by Hwang et al [13] and the nonlinear residual strength model proposed by Yang et al [14]. Here, we will refer to the latter model as the "generalized" nonlinear model. Wahl et al [5] provides a complete description of these models.

3.1 Miner's Rule

Miner's rule defines the damage $\mathbf{D}$, predicted for a time interval T, as

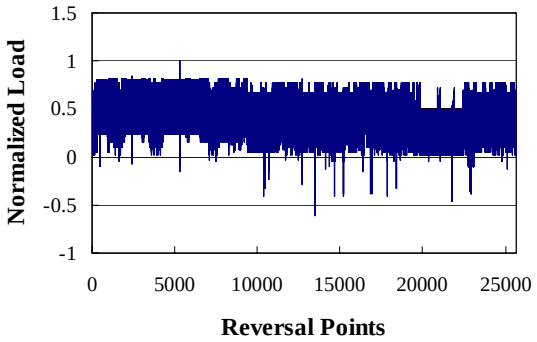

Fig. 6: Normalized WISPERX Spectrum

$$\mathbf{D} = \sum_i \frac{n_i(\sigma)}{N_i(\sigma)} \quad , \tag{6}$$

where n is the number-of-cycles, N is the number-of-cycles to failure and σ describes the stress level of the fatigue cycle. For our case, where we will be using the Goodman diagrams to determine N, σ is divided into two components: the mean stress σ_m and the amplitude σ_A of the stress cycle.

Failure occurs when $\mathbf{D}$ equals one. The predicted service lifetime $\mathbf{L}$, is the time T required for the damage $\mathbf{D}$ (T) to accumulate to a value of one.

3.2 Residual Strength Models

3.2.1 Nonlinear Miner's Sum Model

Miner's rule may also be used to describe the residual strength of composites, see the discussion by Wahl et al [5]. In its general form, the nonlinear Miner's sum model has the following form:

$$\left[\frac{\sigma_R}{\sigma_o}\right]_i = 1 - \sum_{j=1}^{i}\left[\frac{n_j}{N_j}\right]^{\nu} \quad , \tag{7}$$

where $[\sigma_R/\sigma_o]$ is the ratio of the residual strength to the static strength σ_o after step i and the exponent ν is the nonlinear degradation parameter. As discussed in 3.1, N_j is evaluated at the implied stress state (σ_m, σ_A) of n_j.

Failure occurs when the current value of the residual strength $(\sigma_R)_i$ is exceeded by the (i +1) cycle, see the discussion in 3.2.3.

3.2.2 Generalized Nonlinear Model

A generalized nonlinear residual strength model, also see the discussion by Wahl et al [5], takes the form:

$$\left[\frac{\sigma_R}{\sigma_o}\right]_i = \left[\frac{\sigma_i - \sigma_o}{\sigma_o}\right]\left[\frac{n_i + (n_{i-1})^*}{N_i(\sigma_m, \sigma_A)}\right]^{\nu}, \qquad (8)$$

where n_i is the current number of stress cycles and $(n_{i-1})^*$ is the number of previous equivalent cycles determined for the current stress level. The previous equivalent cycles is the number of cycles which would give the residual stress ratio $[\sigma_R/\sigma_o]_i$ if cycled only at $(\sigma_m, \sigma_A)_i$.

If Eq. 8 is rewritten as:

$$\left[\frac{\sigma_R}{\sigma_o}\right]_i = \left[\frac{\sigma_i - \sigma_o}{\sigma_o}\right]\left[\frac{1}{N_i(\sigma_i, R)}\right]^{\nu}\left[n_i + (n_{i-1})^*\right]^{\nu}, \qquad (9)$$
$$= A_i\left[n_i + (n_{i-1})^*\right]^{\nu}$$

then,

$$A_i\left[(n_{i-1})^*\right]^{\nu} = A_{i-1}\left[(n_{i-1})\right]^{\nu} \quad , \text{ or} \qquad (10)$$

$$(n_{i-1})^* = \left[\frac{A_{i-1}}{A_i}\right]^{1/\nu}(n_{i-1}) \quad . \qquad (11)$$

For this analysis, we have computed the residual strength sequentially using Eqs. 8 through 11 for each half-cycle of the sequence.

3.2.3 Residual Strength Ratio

As defined by Eqs. 7 and 9, the residual strength of the composite after i steps for both residual strength models is

$$(\sigma_R)_{i+1} = \left[\frac{\sigma_R}{\sigma_o}\right]_i (\sigma_o)_i \quad . \qquad (12)$$

Failure occurs when the maximum stress of the next cycle $[\sigma_{i+1}]_{MAX}$ exceeds the current tensile residual strength or the minimum stress of the next cycle $[\sigma_{i+1}]_{MIN}$ exceeds the current compressive residual strength:

$$[\sigma_{i+1}]_{MAX} \geq [(\sigma_R)_{i+1}]_{Tensile} \quad ,$$

or (13)

$$[\sigma_{i+1}]_{MIN} \leq -[(\sigma_R)_{i+1}]_{Compressive} \quad .$$

While Eq. 12 is rather obvious, this equation implies that the residual tensile and compressive strength are being reduced proportionally, i.e., the ratio of the residual stress to the static strength is a monotonically decreasing function.

4 Damage Predictions

The models cited in Section 3 are used here to predict the failures of the coupons tested under the WISPERX load spectrum discussed in Section 2. The experimental cycles-to-failure, as a function of the maximum stress in the spectrum, for material DD-16 are shown as the discrete data points in Fig. 7 [5].

4.1 Miner's Rule

The predictions for Miner's rule using the three mean-value Goodman diagrams (see Fig. 2) are shown in Fig. 7a. The linear Goodman diagram predicts the longest lifetimes (cycles-to-failure) and the full Goodman diagram predicts the shortest lifetimes. Notice that the mean fits do not pass through the mean of the data: rather, all three formulations predict service lifetimes that are significantly higher than the measured lifetime.

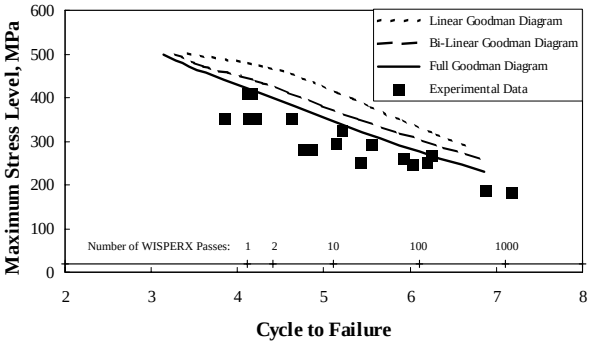

Fig. 7a: Failures Predicted Using the Mean Full Goodman Diagram

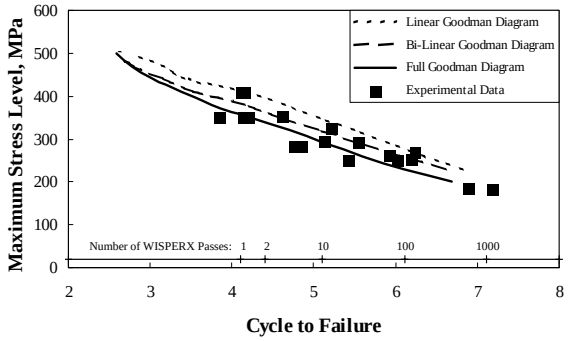

Fig. 7b: Failures Predicted Using the 95/95 Full Goodman Diagram

Fig. 7: Comparison of Experimental Data to Predicted Failure using Linear Miner's Rule

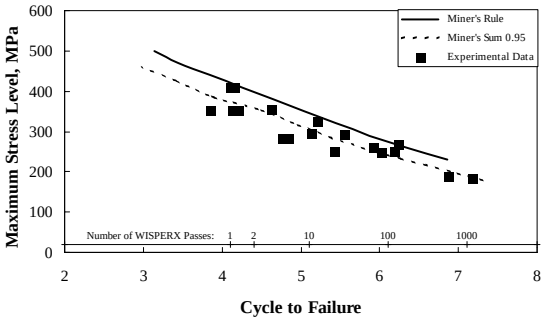

Fig. 8a: Failures Predicted Using the Mean Full Goodman Diagram

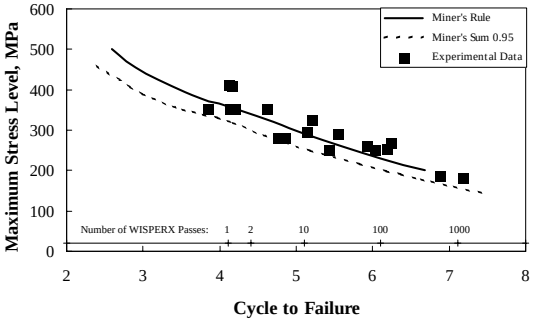

Fig. 8b: Failures Predicted Using the 95/95 Full Goodman Diagram

Fig. 8: Comparison of Experimental Data to Predicted Failure using the Miner's Sum Residual Strength Models

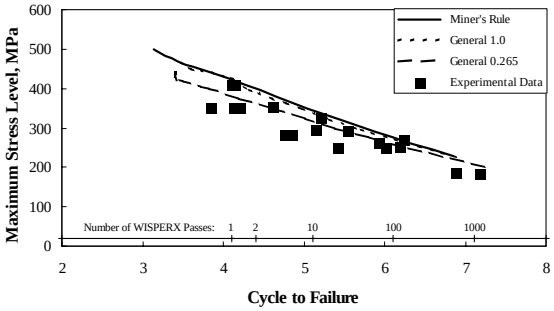

Fig. 9a: Failures Predicted Using the Mean Full Goodman Diagram

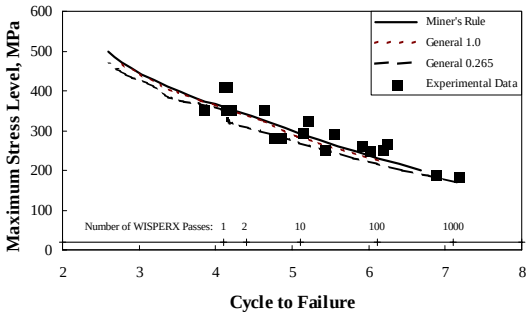

Fig. 9b: Failures Predicted Using the 95/95 Full Goodman Diagram

Fig. 9: Comparison of Experimental Data to Predicted Failure using the Generalized Residual Strength Models

The predictions for Miner's rule using the three 95/95 Goodman diagrams (see Fig. 3) are shown in Fig. 7b. Again, the linear Goodman diagram predicts the longest lifetimes (cycles-to-failure) and the full Goodman diagram predicts the shortest lifetimes. This comparison illustrates that the linear 95/95 Goodman diagram predicts service lifetimes that are higher than the measured lifetime, and, the full 95/95 Goodman diagram predicts lifetimes near the mean of the experimental data.

Thus, Miner's rule does not predict the measured lifetimes very well. Even the 95/95 Goodman diagrams are non-conservative in that they predict longer service lifetimes than those measured in the tests using the WISPERX load spectrum. At best, the full 95/95 Goodman diagram predicts the mean of measured data.

4.2 Residual Strength Models

The two nonlinear residual strength models discussed above were used to predict the lifetimes of the coupons subjected to spectral loading using the WISPERX spectrum. The predictions of these models are summarized in Figs. 8 and 9.

4.2.1 Nonlinear Miner's Sum Model

Note the slopes of the predicted lifetime curves shown in Fig. 7 are consistent with the data, but they are shifted to the right of the data. The nonlinear Miner's sum model described in Eq. 7 shifts the prediction to the left. Using a trial-and-error method, a value of ν = 0.95 was chosen as the best fit to the experientially measured lifetime data using the 95/95 Goodman diagram. The predictions for this residual strength model are shown in Fig. 8.

As shown in this figure, the lifetime curves predicted by Miner's rule with the full Goodman diagrams have been shifted to the left by approximately a half-decade of cycles. These predictions are in very good agreement with the measured lifetimes. Namely, the predicted lifetimes are near the mean of the data, see Fig. 8a, when the mean full Goodman diagram is used

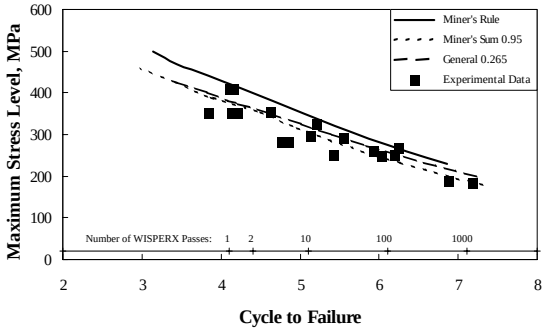

Fig. 10a: Failures Predicted Using the Mean Full Goodman Diagram

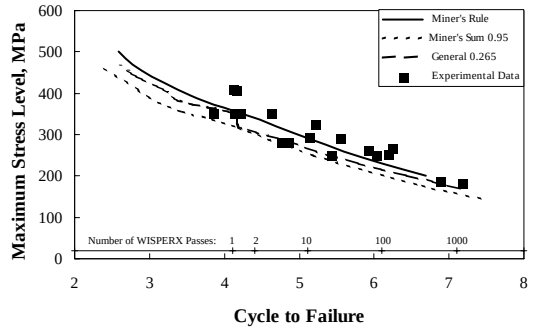

Fig. 10b: Failures Predicted Using the 95/95 Full Goodman Diagram

Fig. 10: Predicted Failure using the Linear and the Nonlinear Models

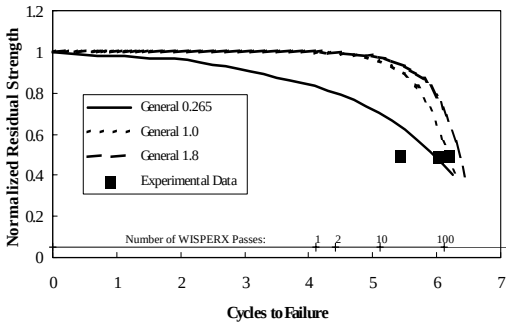

Fig. 11a: Failures Predicted Using the Mean Full Goodman Diagram

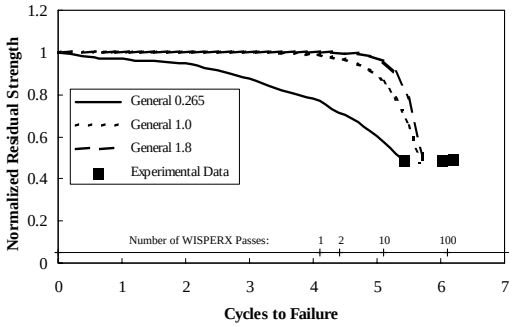

Fig. 11b: Failures Predicted Using the 95/95 Full Goodman Diagram

Fig. 11: Residual Strength using the Generalized Nonlinear Model

and are at or to-the-left-of the measured lifetimes when the 95/95 full Goodman diagram is used, see Fig. 8b.

4.2.2 Generalized Nonlinear Model

The predictions for the generalized nonlinear residual strength model using the mean and the 95/95 full Goodman diagrams (see Fig. 3c and 4c) are shown in Fig. 9. As shown in this figure, for $\nu = 1$, the prediction lies essentially on top of the full-Goodman Miner's rule prediction.

Using the value chosen by Wahl et al [5] of $\nu = 0.265$, the predictions are in general agreement with the data. Namely, the predicted lifetimes are near the mean of the data when the mean full Goodman diagram is used, see Fig. 9a, and are at or to-the-left-of when the 95/95 full Goodman diagram is used, see Fig. 9b. Thus, the generalized nonlinear model with an exponent of 0.265 is also a good predictor of the measured lifetime when used with the full Goodman diagram.

Note the steps in the predicted lifetime, at approximately 425 MPa and $5x10^3$ cycles in Fig. 9a (the beginning of the plot), and at approximately 400 MPa and 10^4 cycles in Fig. 9b. These steps are a direct result of the WISPERX spectrum. As shown in Fig. 6, this load spectrum contains one very large tension cycle after approximately 5000 cycles. This cycle is the cause of failure at both levels of the cited steps: the predicted failure in Fig. 9a occurs at the first occurrence of this relatively large cycle, and it occurs at the second occurrence in Fig. 9b. For this failure, the residual strength is progressively decreasing, until it encounters this relatively large cycle that exceeds the current residual strength of the composite. If this plot had been constructed with finer resolution, other, similar steps would be present.

4.2.3 Residual Strength Comparisons

Figures 10 and 11 illustrate the predicted residual failure strength of the composite using the linear Miner's rule and the two nonlinear residual strength models.

The major difference between the three models is illustrated in Fig. 11. As shown in this figure, the loss of residual strength as fatigue cycles accumulate is very different for the three models. For Miner's rule, the composite retains its strength for most of its lifetime, and, as failure approaches, its residual strength drops precipitously. For the nonlinear Miner's sum, with $\nu = 0.95$, the residual strength curve maintains the same form, but is shifted to the left, i.e., it predicts a shorter lifetime. For the generalized nonlinear residual strength model with $\nu = 0.265$, the residual strength starts decreasing almost immediately and continues to decrease until failure occurs.

5 Concluding Remarks

The updated Goodman diagrams presented here have been developed using the MSU/DOE Fatigue Data Base [2]. The six diagrams constructed here are based upon S-N data obtained at thirteen different R-values. Separate Goodman diagrams were constructed using both the mean and the 95/95 representations of the data. The effects of these improved representations of the behavior of fiberglass composites were illustrated using coupons tested to failure using the WISPERX load spectrum. This load spectrum is primarily a tensile load spectrum. These comparisons illustrate that when a Miner's rule damage criterion is used the mean fits of the data do not predict failure very well, while the 95/95 fits predict failures near the mean of measured data. Both a nonlinear Miner's sum model and a generalized nonlinear residual strength model, when used with the 95/95 full Goodman diagram, predict the lower bound of the measured data very well, and when used with the mean full Goodman diagram, predict the mean lifetime very well.

6 References

[1] Mandell, J.F., D.D. Samborsky, N.K. Wahl, and H.J. Sutherland, "Testing and Analysis of Low Cost Composite Materials Under Spectrum Loading and High Cycle Fatigue Conditions," Conference Paper, *ICCM14*, Paper # 1811, SME/ASC, 2003.

[2] Mandell, J.F., and D.D. Samborsky, *DOE/MSU Composite Material Fatigue Database: Test Methods, Materials, and Analysis*, Report SAND97-3002, Sandia National Laboratories, Albuquerque, NM, 1997.

[3] Ten Have, A.A., *WISPER and WISPERX: Final Definition of Two Standardized Fatigue Loading Sequences for Wind Turbine Blades*, NLR-TP-91476U, National Aerospace Laboratory NLR, Amsterdam, the Netherlands, 1992,

[4] Sutherland, H.J., and J.F. Mandell, "Effect of Mean Stress on the Damabe of Wind Turbine Blades," *2004 ASME Wind Energy Symposium*, AIAA/ASME, 2004.

[5] Wahl, N.K., J.F. Mandell, D.D. Samborsky, *Spectrum Fatigue Lifetime and Residual Strength for Fiberglass Laminates*, Report SAND2002-0546, Sandia National Laboratories, Albuquerque, NM, 2002.

[6] Mandell, J.F., D.D. Samborsky, and D.S. Cairns, *Fatigue of Composite Materials and Substructures for Wind Turbine Blade*, Contractor Report SAND2002-077, Sandia National Laboratories, Albuquerque, NM, 2002.

[7] Mandell, J.F., D.D. Samborsky, D.W. Combs, M.E. Scott and D.S. Cairns, *Fatigue of Composite Material Beam Elements Representative of Wind Turbine Blade Substructure*, Report NREL/SR-500-24374, National Renewable Energy Laboratory, Golden, Co, 1998.

[8] Echtermeyer, T., E. Hayman, and K.O. Ronold, "Estimation of Fatigue Curves for Design of Composite Laminates," *Composites-Part A (Applied Science and Manufacturing)*, Vol. 27A, No. 6, 1996, p. 485.

[9] Sutherland, H.J., and P.S. Veers, "The Development of Confidence Limits For Fatigue Strength Data," *2000 ASME Wind Energy Symposium*, AIAA/ASME, 2000, pp. 413-423.

[10] ASTM, E739-91, *Standard Practice for Statistical Analysis of Linear or Linearized Stress-Life (S-N) and Strain-Life (e-N) Fatigue Data*, ASTM, Conshohocken, PA.

[11] Kensche, C.W., "Effects of Environment," *Design of Composite Structures Against Fatigue*, R. M. Mayer, ed., Mechanical Engineering Pub. Limited, Bury St Edmunds, Suffolk, UK, 1996, pp.65-87

[12] Nijssen, R.P.L, D.R.V. van Delft and A.M. van Wingerde, "Alternative Fatigue Lifetime Prediction Formulations for variable Amplitude Loading," *2002 ASME Wind Energy Symposium*, AIAA/ASME, pp. 10-18.

[13] Hwang, W., and K.S. Han, "Cumulative Damage Models and Multi-Stress Fatigue Life Prediction," *J. of Composite Materials*, Vol. 20, March, 1986, pp. 125-153.

[14] Yang, J.N., D.L. Jones, S.H. Yang, and A. Meskini, "A Stiffness Degradation Model for Graphite/Epoxy Laminates," *J. of Composite Materials*, Vol. 24, July, 1990, pp. 753-769.